(FT) catalyst. However, ruthenium has been similarly as nickel mostly used in combination catalysts because it is expensive (two orders of magnitude more expensive than cobalt) and has much higher range of optimum working pressures compared to iron or cobalt. Until today thousands of different catalyst formulations have been tested and hundreds of active catalysts have been proposed with iron and cobalt based catalysts being the most common commercially. Recently more studies have been directed toward the cobalt based FT catalysts because of their high activity and modular selectivity. Iglesia (1997) and Oukachi et al. (1999) reviewed various cobalt based FT catalysts. Since catalyst activity and selectivity (which are affected by catalyst porosity, tortuosity, density which is usually greater than 5 gm/cm^3, surface composition and structure, wetability, etc.) are determined by catalyst chemical composition, type of carrier (catalyst support), catalyst preparation process, activation procedure, etc. The FT catalyst properties vary noticeably.

Traditionally the most often used support (binder) of FT catalysts have been silica (SiO_2) and alumina (Al_2O_3) (density between 1.5 to 3 gm/cm^3). Some early German catalysts used the Kieselguhr. In addition to these supports, titania (TiO_2), magnesia (MgO), active carbon and zeolits (e.g. ZSM-5) have been somewhat less frequently used (Storch et al., 1951).

Hence, hydrodynamics obtained using one catalyst may not represent a general information for all the catalyst types. Using only FT catalyst supports for hydrodynamics investigation does not either provide representative information due to the difference in the particle physical and mechanical properties. Therefore, in the open literature, most of the investigations on the hydrodynamics of cold-flow model slurry bubble column reactors have been performed using glass beads of different sizes and air-water/hydrocarbon system (Ong et al., 2000).

3. PREPARATION OF THE EXPERIMENTAL FACILITIES AND THE ADVANCED MEASUREMENT TECHNIQUES

Preparation has been made to the experimental facilities and to the measurement techniques that will be used for the hydrodynamics investigation of the FT slurry bubble column reactors. These facilities, techniques and their preparation are summarized below.

3.1 High pressure and high temperature 2" diameter slurry bubble column

The schematic diagram of the high pressure and high temperature slurry bubble column is shown in Figure 3.1. The actual photo of the column is shown in Figure 3.2. The column is made of stainless steel and is 80 cm in height and 8.08 cm in diameter. Three pairs of plane windows made of quartz are installed on the column; each window is 15 mm wide and 180 mm long. These windows allow viewing throughout the entire test section of the column. The present experiments are conducted at pressures up to 21 Mpa and temperatures up to 180°C. The pressure is controlled by a back pressure regulator installed at the outlet of the bed. The set-up has been tested for leakage and operation.

3.2 High pressure 6 inch diameter slurry bubble column

High pressure 6" slurry bubble column experimental setup (Figure 3.3) is designed to support the maximum operating pressure of 200 psig at room temperature. Compressed air is used as gas phase and is supplied from the compressor with working pressure of 185 psig at the maximum flowrate of 310 SCFM. Air passes through an air filter, pressure regulator, flowmeter setup (4 rotameters of increasing range in parallel) and enters through a check valve (to prevent liquid/slurry phase back flow) into distributor chamber of the bubble column. Air exits the column through a demister, passes through the back pressure regulator (that controls column operating pressure) and vents to atmosphere. A laboratory scale 16.15 cm (6") diameter stainless steel bubble column is used in all experiments. Column design enables easy removal of the distributor chamber and sparger replacement. Two similar column designs are used to suit all the needed experiments. The first one, designed for CARPT/CT experiments, is a smooth 6" column equipped with just two probe ports (1") at each end of the column. The second one (Figure 3.4), for probe measurements, is the same 6" column equipped with an array of additional 15 probe ports (1") and 6 (12"H x 1½"W) view ports. View ports mounted by three at radially opposite sides are staggered to cover the middle and the top part of the column. The batch of slurry constitutes of the selected solvent as the liquid phase and the selected solid phase.

Both 6" columns have been installed and tested.

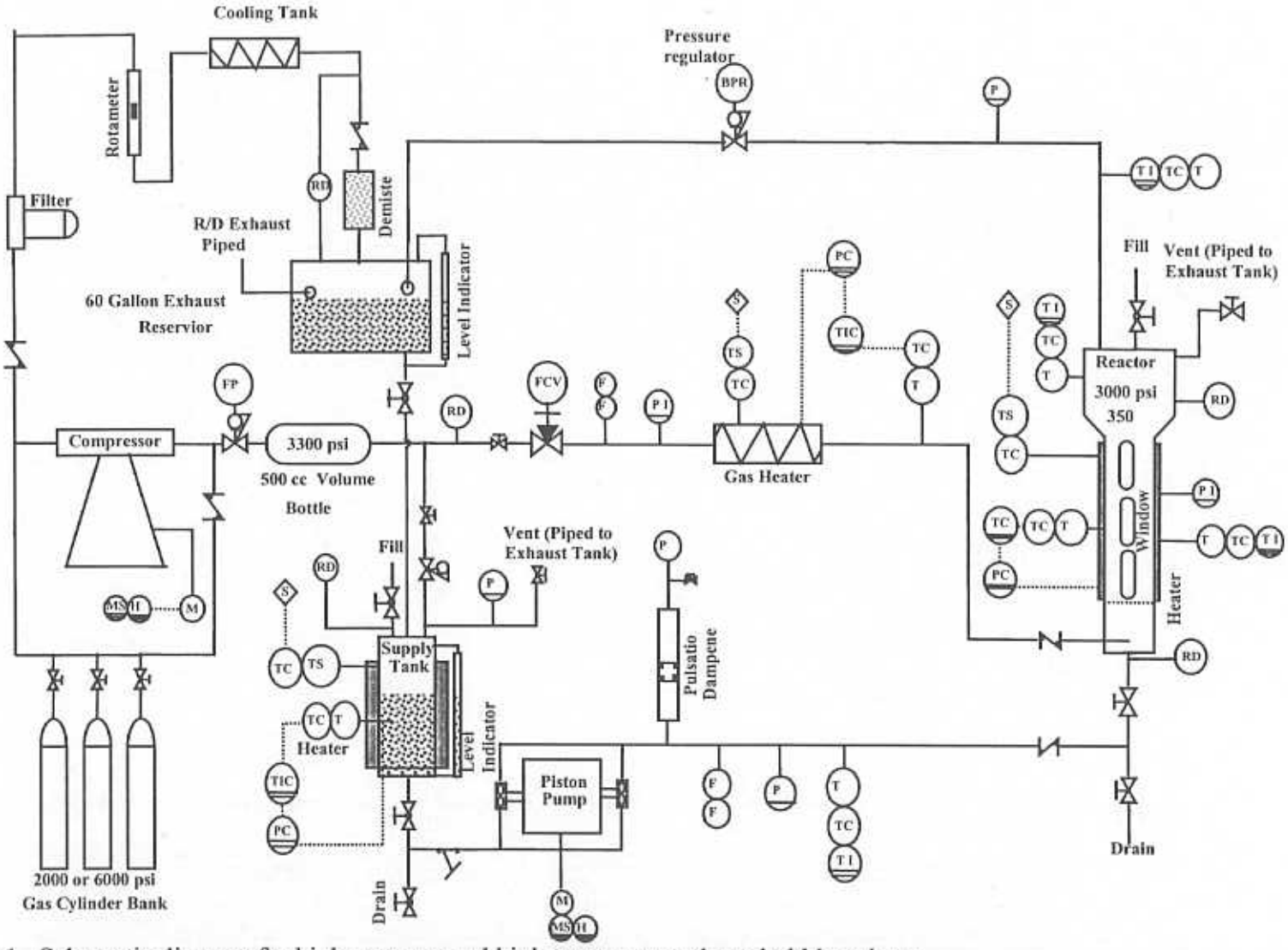

Figure 3.1. Schematic diagram for high pressure and high temperature slurry bubble column.

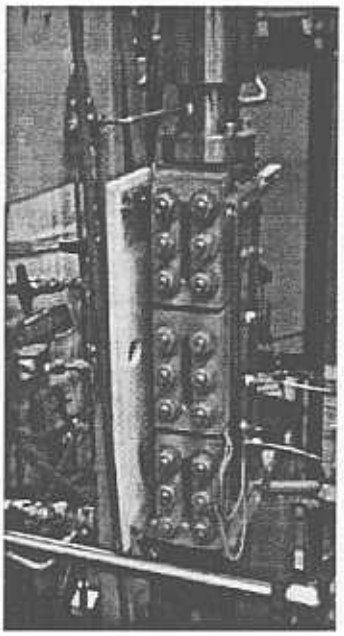

Figure 3.2. Photo of high pressure and high temperature 2" diameter slurry bubble column.

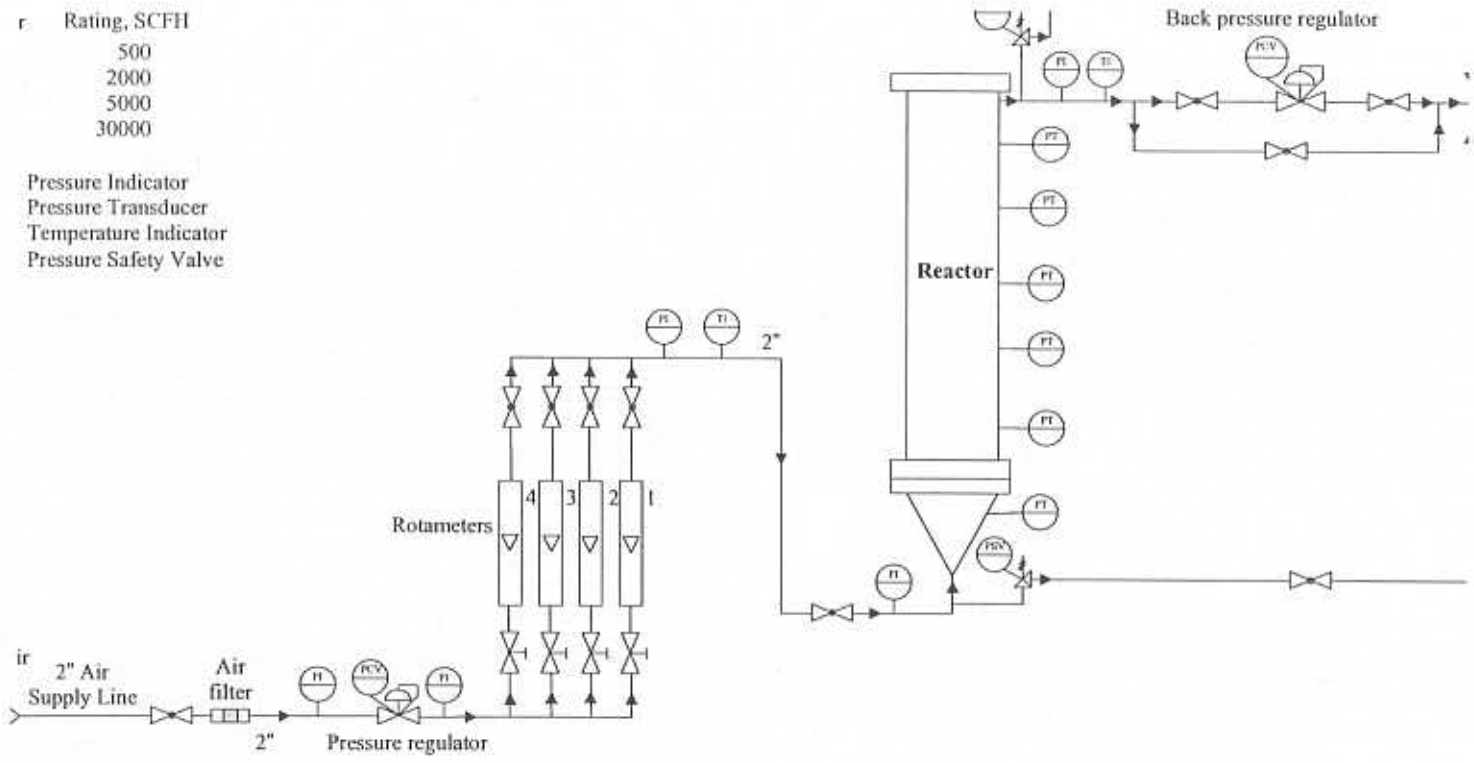

Figure 3.3. Gas flowsheet for the high pressure 6 inch diameter bubble column

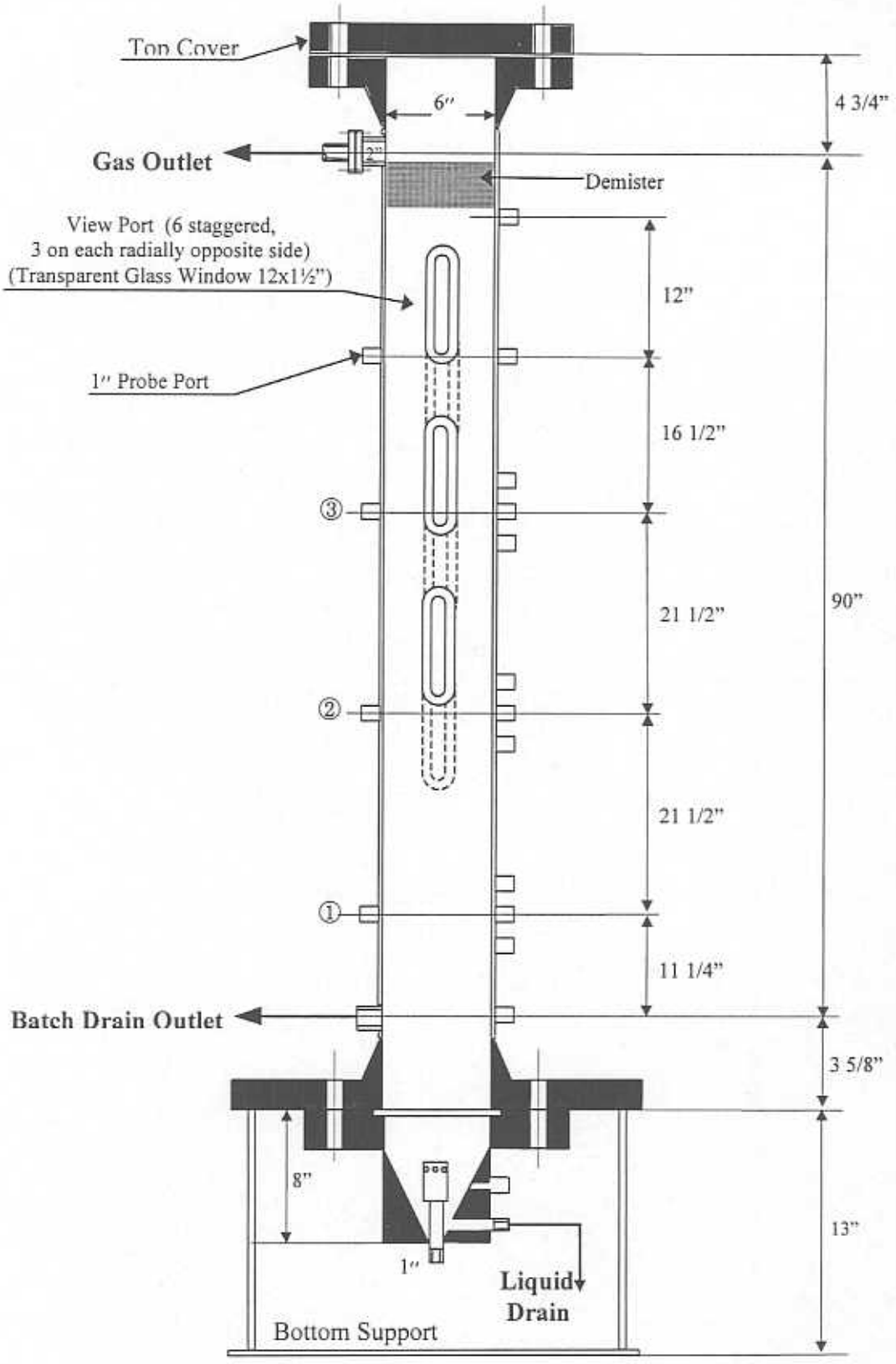

Figure 3.4. High pressure bubble column (probe measurement variation) design.

3.3 Particle Image Velocimetry (PIV)

The high speed PIV or LDA system, will be used in this project. Figure 3.5 shows a schematic diagram of the PIV system. The CCD image pick-up on the high frame rate camera features 765 pixels across by 246 lines. Camera speed can be selected up to 480 pictures per second. The camera is equipped with an asynchronous variable electronic shutter ranging from 1/60 second to 1/10000 second. The CCD image from the high frame rate camera can be simultaneously digitized by the high frame rate / high capacity frame grabber. The frame grabber is equipped with 40 MHz max pixel clock and 256 MB on board memory. Moreover, the high frame rate camera can be connected the high frame rate video recorder (240 pictures per second) for further study. A 4-watt argon ion laser system is utilized as a light source. A fiber optic cable is used to carry the laser light from the laser source to the test column. A cylindrical lens arrangement attached to the end of the fiber optic cable creates a laser sheet of thickness 5 mm.

3.4. Laser Doppler Anemometer (LDA)

The Laser Doppler Anemometer was invented by Yeh and Cummins in 1964. It is capable of non-intrusive velocity measurements in fluid dynamics in both gas and liquid phases. It has up to three velocity components with high accuracy and high spatial resolution due to small measurement volume. The basic components of an LDA include a continuous wave laser, a traverse system, transmitting and receiving optics and a signal conditioner and a signal processor. Figures 3.6 and 3.7 show the setup of the LDA system and the transmitting optics on the traverse system respectively. A 300-mW air-cooled argon-ion laser and a beam separator are used to generate two pairs of beams of known wavelengths of 514.5 and 480 nm. The light is transmitted through a fiber optic cable and a probe with 3.40 and 3.22 μm and measurement volumes of 0.164 X 0.164 X 2.162 mm and 0.156 X 0.156 X 2.05 mm for the 514.5 and 480-nm wavelengths respectively. The scattered light is collected with a detector and processed with a signal processor.

The principle of the operation follows that when a particle passes through the intersection volume formed by the two coherent laser beams, the scattered light received by a detector has components from both beams. The components interfere on the surface of the detector. Due to changes in difference between optical path lengths of the two components this interference produces pulsating light intensity as the particle moves through the measurement volume.

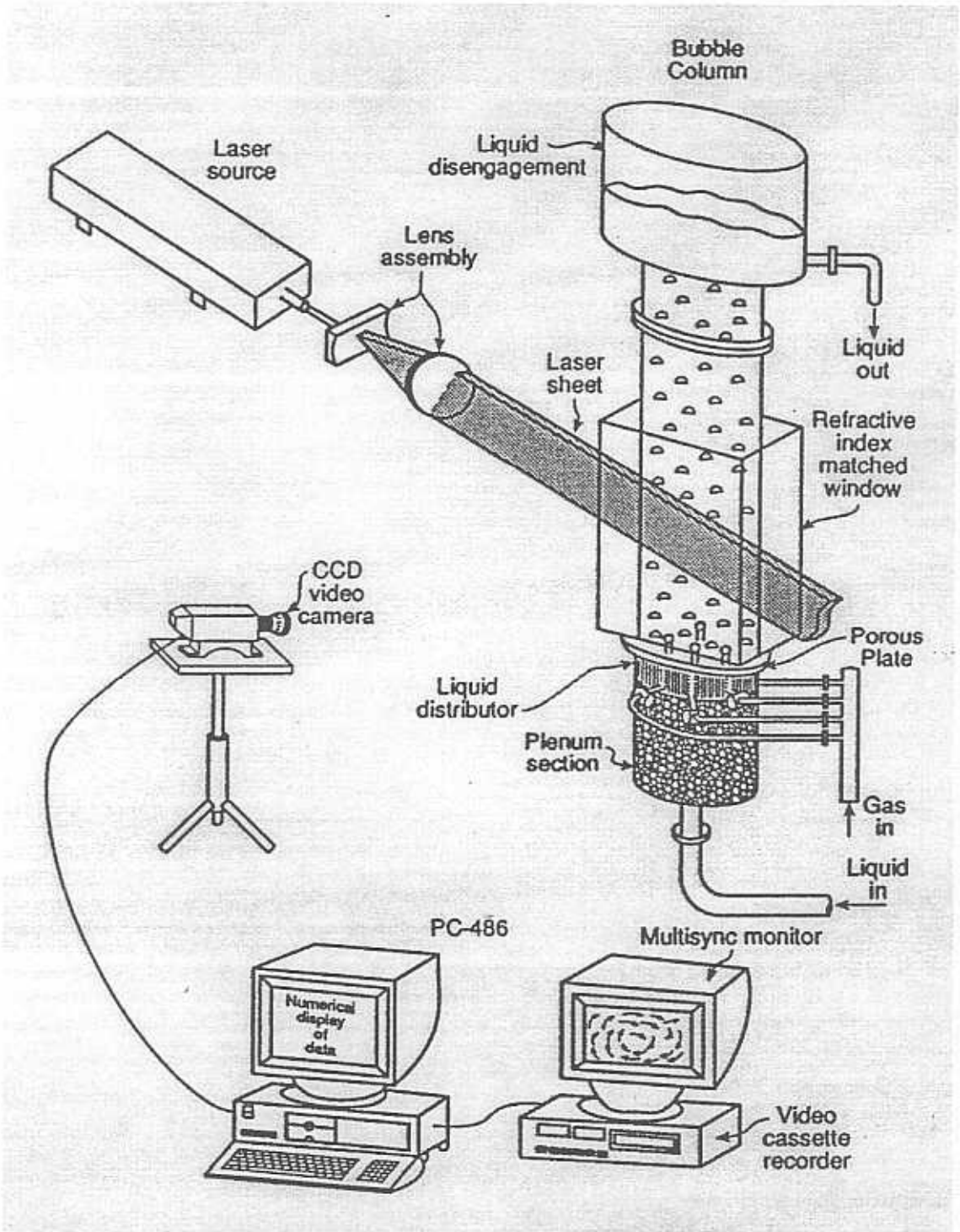

Figure 3.5. Schematic diagram of PIV system

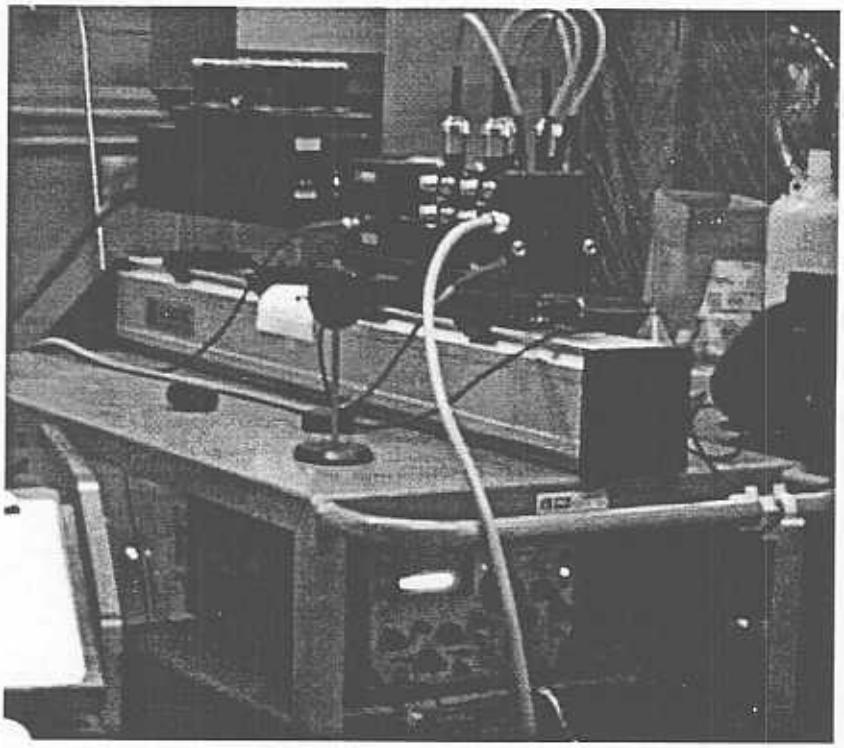

Figure 3.6. Laser Doppler Anemometer Setup.

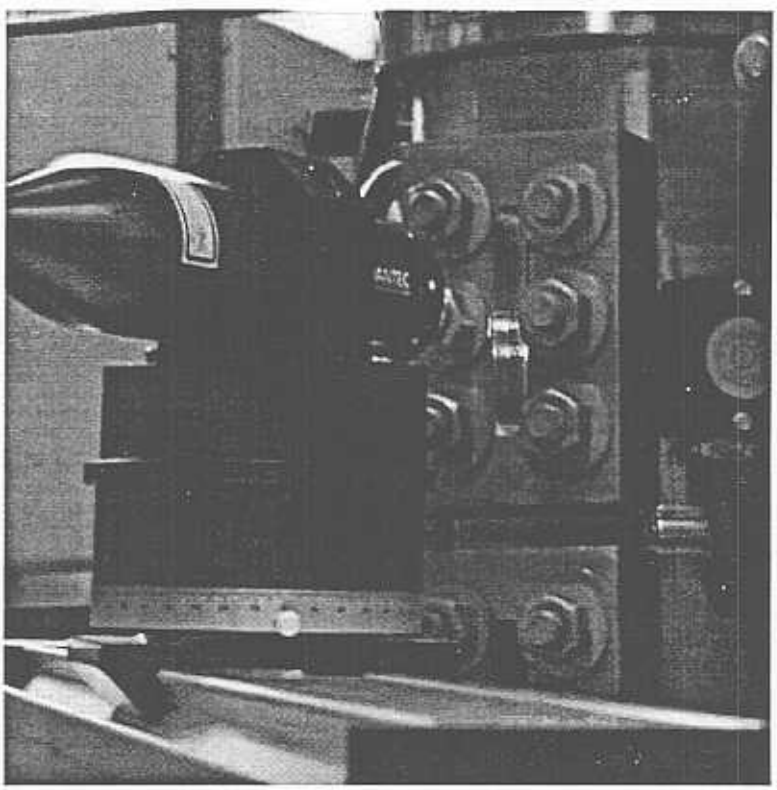

Figure 3.7. Transmitting optics applied on traverse system

3.5 Computer Automated Radioactive Particle Tracking (CARPT)

CARPT is a technique for tracking of a single radioactive tracer particle by detecting the intensity distribution of emitted γ-rays (Figure 3.8). It consists of a number of scintillation detectors (16-32) to monitor the motion of a single small radioactive particle in multiphase systems. This technique has been used extensively at Washington University (Chemical Reaction Engineering Laboratory) to measure in a non-invasive manner the flow pattern and turbulent parameters of different multiphase flow reactors. A fully wettable, neutrally buoyant particle is used to simulate the motion of the liquid in gas-liquid system and particle of the size and density of the solids used is employed for monitoring the motion of solids in two and three phase fluidized beds and other multiphase systems. Scandium 46 at activities of about 200 – 500 μci is used in a composite made tracer particle. Collected data for the tracer particle location in time is used to compute the tracer particle velocity and "turbulent" parameters. Precise calibration and good radioactive particle tracking are essential in obtaining accurate and reproducible CARPT data. In this work the assessment of solids velocities and "turbulent" parameters in a FT slurry bubble column is sought. Thus, the radioactive tracer particle should, as closely as possible, track the solids present in the system. To accomplish this the tracer particle should be comparable in size and density to the solid phase particles. Scandium is a highly reactive rare earth metal whose reactivity increases with increase in surface area per unit volume (decrease of diameter). To resolve the issue of the reacting scandium tracer particle we have developed a new technique for coating and protecting the minute size tracking particles. A tracer scandium Sc45 particle of required diameter is protected with a thin coating of Parylene N, an extremely inert derivative of poly p-xylene with excellent thermal and mechanical properties. The coated Scandium particle is then irradiated in a nuclear reactor. The resulting radioactive scandium Sc46 particle (strength of up to 200 μCi and half-life of 83 days) with a total diameter within the solid phase particle size range is thus used as a tracer particle. Since the density of Parylene N is 1.11 g/cm^3, application of different coating thickness lower the overall particle density from 2.99 g/cm^3 (of pure scandium) to about 2 g/cm^3.

A detailed experimental setup and calculation procedure for CARPT experiments is given by Degaleesan (1997). In-situ calibration of detectors will be performed under the desired operating conditions using a calibration device that is operated under high pressure. CARPT data (tracer particle position in time) acquired over sufficiently long time, to insure enough particle occurrences in each column cell and good time/ensemble averaging, is used for calculation of the time averaged solids:

a) velocities,
b) "Reynolds" stresses,
c) "turbulent" kinetic energy and
d) eddy diffusivities.

A sample of the CARPT results in an air-water-glass beads system in a 6" bubble column is presented in Figure 3.9 (Rados, 1999).

This unique technique is essential for validation of hydrodynamic models used in design and scale-up and testing the effect of different design and operation variables (e.g. pressure, gas velocity, distributor design, internals, etc.) on the flow patterns in FT slurry bubble column reactors.

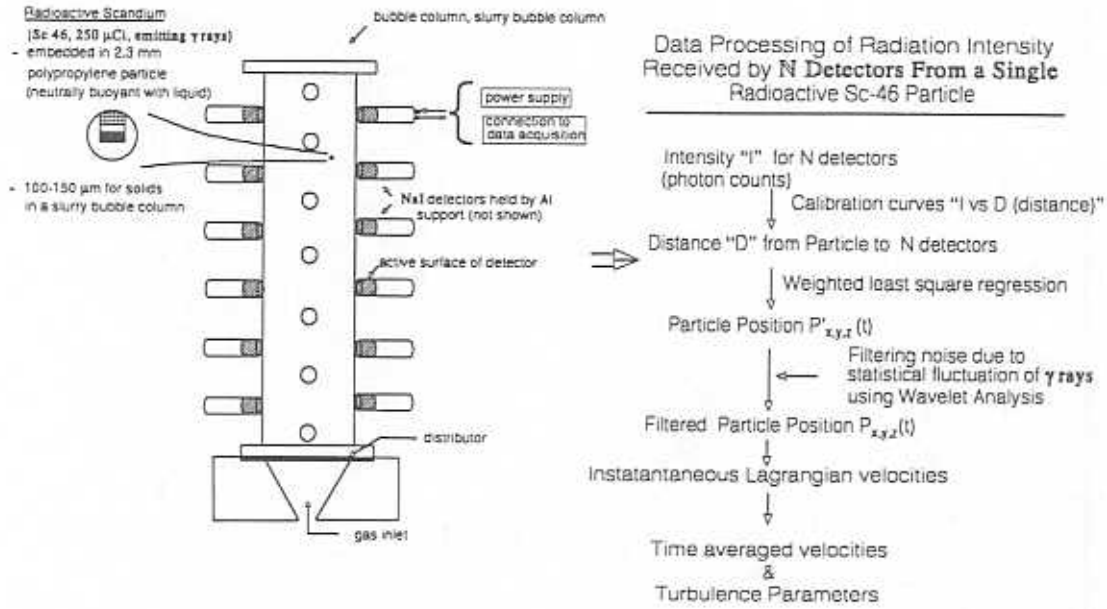

Figure 3.8. Configuration of the CARPT experimental setup.

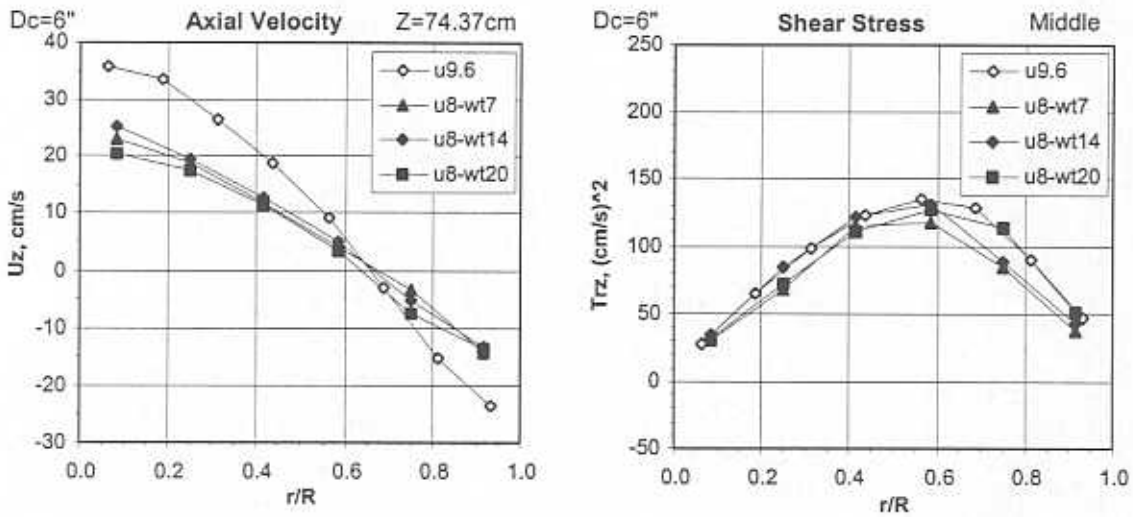

Figure 3.9. Time and azimuthally averaged axial velocity and shear stress radial profiles.
u8-wt14 denotes gas velocity of 8 cm/s and 14 wt.% solids loading. (Sannaes, 1997).

3.6 *Computed Tomography (CT)*

CT is a technique for measurement of the cross-sectional phase holdup distribution in multiphase systems (Figure 3.10).

The CT technique has been extensively implemented at Washington University on various multiphase flow systems. It consists of an array of detectors and an opposing source rotate together around the object to be scanned. The scanner uses a cesium-137 encapsulated γ–ray source with activity of ~ 85 mCi. The array of detectors and the source are mounted on a gantry which can be rotated about the object to be scanned through a step motor. The entire system is completely automated to acquire the data required for the reconstruction of the phase distribution in a given cross-section. The Estimation-Maximization algorithm for image reconstruction has been implemented. It is based on maximum likelihood principles and takes into account the stochastic nature of the projection measurements.

Single source CT is used for phase holdup reconstruction in two phase (e.g., gas-liquid) systems. Theoretically, dual source CT is capable of resolving the holdups in three phase systems (e.g., gas-liquid-solid). However, because of numerical error accumulation dual source CT reconstruction of holdup profiles is still not practical (Daly et al., 1996). In this work we utilize a new combination of measurement techniques CT/DP/CARPT that can be used to calculate holdup profiles of all three phases in a slurry system at all operating conditions including high pressure, high SGV and high solids loading (Rados, 1999).

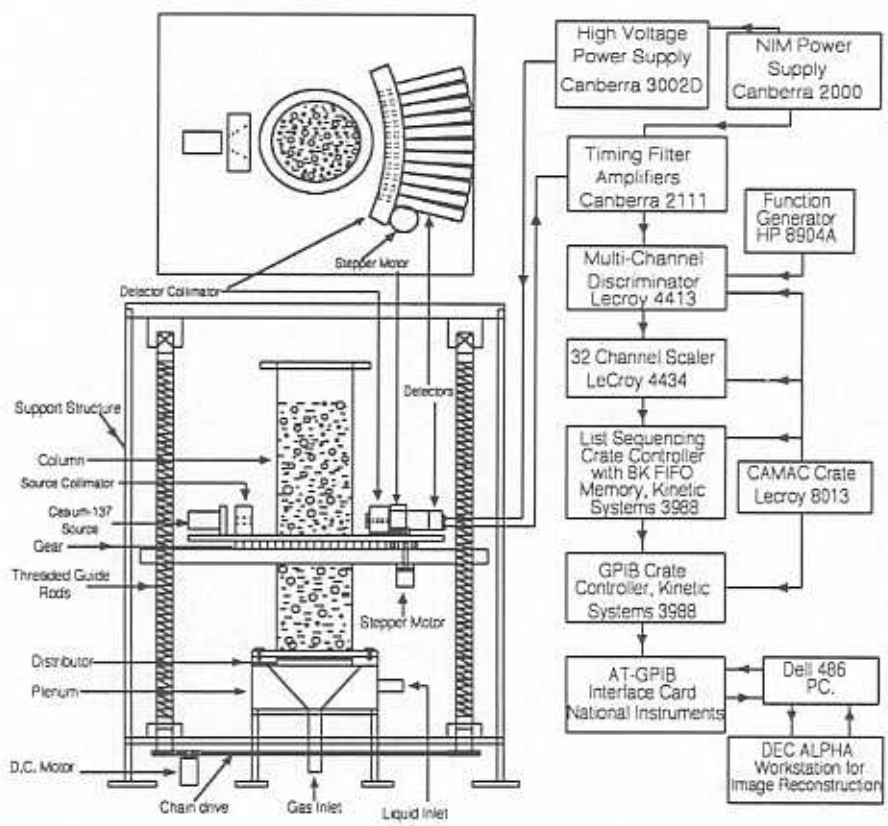

Figure 3.10: Configuration of the CT experimental setup (Kumar, 1994).

For a single γ radiation source, absorbance A over the path l is equal to:

$$A = -\ln\frac{I}{I_0} = \sum_l (\rho\mu)_{ij} l_{ij} \tag{3.1}$$

where I_0 is the intensity of radiation emitted by the source, I is the intensity of radiation received by the detector. Σ indicates the summation of the volumetric attenuation $(\rho\mu)_{ij}$ of each cell ij multiplied by the path length in that cell l_{ij} along the path l, through which the radiation beam passes on its way from the source to the detector. If sufficiently large number of the scans of the operating column are taken from different directions (projections) then the volumetric attenuation in each cell $(\rho\mu)_{ij}$ can be calculated. To get the holdup distribution we have to measure the absorbance A_K for an empty column (K=G), for a column filled with liquid (K=L), for a column with solids and gas in voids between solid particles (K=GS) and for a column in operation with the gas-liquid-solid slurry (K=GLS). For each of these situations the detected intensity of radiation I_K and hence the measured absorbance A_K is different. Since the flow is time dependent larger number of acquired projections than cells (#equations >> #unknowns, over sampling) will yield more accurate time averaged attenuation coefficients (better statistics). In general I_0 is unknown and because of that the intensity of radiation I_K must be normalized with the intensity of radiation detected in the column containing only the gas phase I_G. In addition the intensity I_K must be corrected for the background (room) radiation intensity $I_{K,bck}$. This yields the following equation for A_K:

$$A_K = -\ln\frac{I_K - I_{K,bck}}{I_G - I_{G,bck}} = \sum_l \left[(\rho\mu)_{K,ij} - (\rho\mu)_{G,ij}\right] l_{ij} \tag{3.2a}$$

One defines relative volumetric attenuation as:

$$R_{K,ij} = (\rho\mu)_{K,ij} - (\rho\mu)_{G,ij} \tag{3.2b}$$

For the column containing packed bed of solids (uniform holdup of ε_S^0) and gas in voids between the solids particles the volumetric attenuation coefficient in cell ij is equal to:

$$(\rho\mu)_{GS,ij} = (\rho\mu)_{S,ij}\varepsilon_S^0 + (\rho\mu)_{G,ij}\left(1-\varepsilon_S^0\right) \tag{3.3}$$

Substitution of eq. (3.2b) into eq. (3.3) (written for the gas-solid system, K = GS) after some manipulation yields the local solids volumetric attenuation coefficient:

$$(\rho\mu)_{S,ij} = \frac{R_{GS,ij} + (\rho\mu)_{G,ij}\varepsilon_S^0}{\varepsilon_S^0} \tag{3.4}$$

Similarly, for a slurry system:

$$(\rho\mu)_{GLS,ij} = (\rho\mu)_{G,ij}\varepsilon_{G,ij} + (\rho\mu)_{L,ij}\left(1-\varepsilon_{G,ij}-\varepsilon_{S,ij}\right) + (\rho\mu)_{S,ij}\varepsilon_{S,ij} \tag{3.5}$$

Eq. (3.5) combined with eq. (3.2b) (written for liquid, K=L and slurry, K=GLS) and eq. (3.4) yields the expression for local gas holdup (cell ij):

$$\varepsilon_{G,ij} = \frac{R_{GS,ij}\dfrac{\varepsilon_{S,ij}}{\varepsilon_S^0} + R_{L,ij}\left(1-\varepsilon_{S,ij}\right) - R_{GLS,ij}}{R_{L,ij}} \tag{3.6}$$

Clearly in order to close the system of equations we need one more equation for local solids holdup $\varepsilon_{S,ij}$. In dual source CT one more equation of the form (3.2) can be written for the other γ source. In this work the additional equation is generated from DP and CARPT measurements:

$$-\frac{1}{g}\frac{\Delta P}{\Delta z} = \rho_G\overline{\varepsilon_G} + \rho_L\left(1-\overline{\varepsilon_G}-\overline{\varepsilon_S}\right) + \rho_S\overline{\varepsilon_S} \qquad \text{DP} \qquad (3.7)$$

$$\varepsilon_{S,ij} = n_{S,ij}\frac{\overline{\varepsilon_S}}{\overline{n_S}} \qquad \text{CARPT} \qquad (3.8)$$

DP equation (3.7) assumes fully developed flow, no axial holdup profiles and negligible wall shear stress in the section Δz. Fully developed flow in slurry systems is usually reached at heights above two column diameters. Axial holdup profiles can be neglected over small Δz distances and the wall shear stress has been shown to be negligible compared to the pressure drop (Fan, 1989, less than 1%). CARPT equation (3.8) states that the volume averaged number of radioactive tracer particle occurances in the specific cell $n_{S,ij}$ is proportional to the solids holdup in that cell assuming that the radioactive tracer particle completely resembles solid phase particles and that all cells in considered cross plane are well perfused and readily accessible to the radioactive tracer particle (Moslemian et al., 1992). This assumption is justified in churn turbulent regime. Finally, the combination of eq. (3.7) and (3.8) yields the expression for the local solids holdup (cell ij):

$$\varepsilon_{S,ij} = \frac{-\dfrac{1}{g}\dfrac{\Delta P}{\Delta z} - \rho_G\overline{\varepsilon_G} - \rho_L\left(1-\overline{\varepsilon_G}\right)}{\rho_S-\rho_L} \times \frac{n_{S,ij}}{\overline{n_S}} \tag{3.9}$$

Using the following iterative procedure the holdup profiles of all three phases can be calculated.

1) Guess the cross-sectional average solids holdup. The initial guess is based on the calculation of the cross-sectional average solids holdup from the overall gas holdup measurements and nominal solids loading (v_{S0}, volume of solids per volume of slurry suspension initially charged into the column) using the equation $\overline{\varepsilon_S} = v_{S0}(1-\overline{\varepsilon_G})$.
2) Using eg. (3.8) calculate the solids holdup in each cell.
3) Using eq. (3.6) calculate the gas holdup in each cell.
4) Calculate the cross-sectional average gas holdup.
5) Using eq. (3.9) calculate the solids holdup in each cell.
6) Calculate the cross-sectional average solids holdup.
7) Compare the calculated and previous values (initial guess in the first iteration) of the cross-sectional average solids holdup.
8) Using the solids holdups in each cell recalculated in step 5 repeat the steps 3 through 7 until specified tolerance is achieved (convergence).

3.7 *Physical properties measurements techniques*

Most industrial processes are operated at extreme conditions with high temperatures and pressures, while most research reports have been focused on ambient conditions. It is known that the bubble formation process will be affected by the properties of gas and liquid, the diameter of nozzle, gas chamber pressure and the gas flow rate. The bubble interaction is function of the initial bubble size, bubble rise velocity and bubble breakup and coalescence. However, all of these are relative to gas and liquid physical properties. It is essential to know how the physical properties change with pressure and temperature for an individual system. Therefore, it is possible to characterize the transport phenomena of bubble columns operated under high pressure and high temperature based on the physical properties of the phases rather than the operating pressure and temperature.

3.7.1. *Density measurement*

The hydrostatic weighing method is adopted to measure the liquid density at elevated pressures and temperatures. A cylindrical aluminum tube of 0.305 m in length and 7.14 mm in outside diameter, shown in Figure 3.11, is submerged in the liquid. The volume of the tube above the liquid surface varies with the liquid density. Specifically, the liquid density relates to the tube volume above the liquid surface based on the Archimedes principle:

$$S[\rho_l l_1 + \rho_g (l - l_1)] = (W_1 + W_2) + S_1 \rho_g l_2 \qquad (3.10)$$

where W_1 and W_2 are the mass of the aluminum tube and metal weight respectively; ρ_l and ρ_g are the densities of liquid and pressurized nitrogen gas respectively; and S and S_1 are the cross-sectional areas of the tube based on the outer and inner diameters respectively.

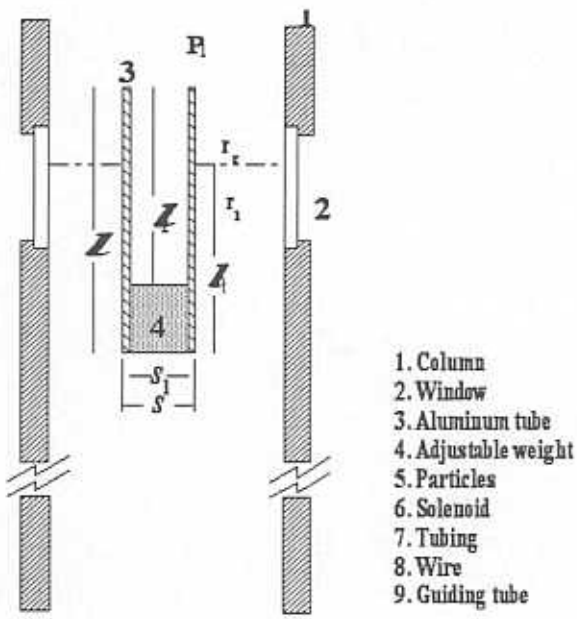

Figure 3.11. Density measurement apparatus setup.

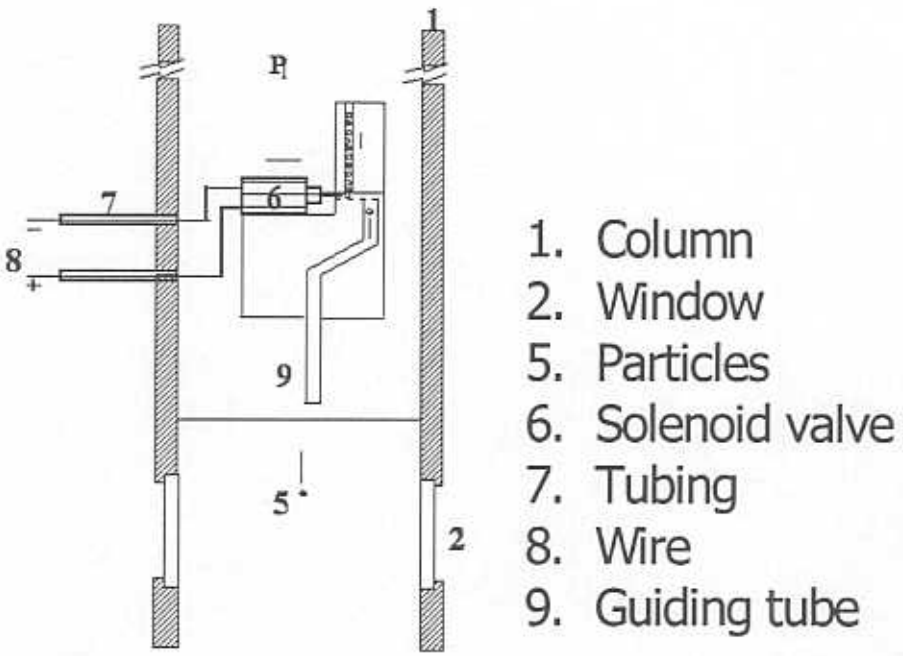

Figure 3.12. Viscosity measurement apparatus setup.

3.7.2. Viscosity measurement

The viscosity of the liquid under elevated pressures and temperatures is determined using the falling ball technique shown in Figure 3.12. A ball dropping device is used to release spherical particles into the column. The falling process is recorded by a CCD camera with an infinity lens situated outside the window. At steady state, the terminal velocity of the falling ball can be calculated from the falling distance (L) and the elapsed time (Δt). The particle size is selected in such a way that the Reynolds number is within the Stokes or intermediate region.

3.7.3. Surface tension measurement

The bubble emergent method is applied to measure the surface tension at varying pressures (up to 21 MPa) and temperatures (up to 250°C). A steel tube is inserted vertically into the column and submerged in the liquid, as shown in Figure 3.13. Video of the bubble generation process is recorded by a high resolution (800 X 490 pixel) CCD camera with an infinity lens. The gas-liquid boundary in Cartesian coordinates of the bubble before detachment is determined. The boundary coordinates are then submitted into the program developed by Jennings and Pallas (1988), from which the surface tension is calculated.